J. Fluid Mech. (1988), *vol.* 187, *pp.* 179–196
Printed in Great Britain

Large deformations and burst of a capsule freely suspended in an elongational flow

By X. Z. LI, D. BARTHES-BIESEL AND A. HELMY
Division de Biomécanique (U.A. CNRS 858), Université de Technologie de Compiègne, BP 649, 60206 Compiègne, France

(Received 17 October 1986 and in revised form 13 May 1987)

An axisymmetric capsule, consisting of an incompressible liquid droplet, surrounded by an infinitely thin elastic membrane having a Mooney constitutive behaviour, is suspended into another incompressible Newtonian liquid subjected to an elongational shear flow. The motion and the deformation of the capsule are determined numerically by means of a boundary-integral technique. It is thus possible to reach large deformations, and to study the influence of the initial geometry of the particle, as well as that of the constitutive behaviour of the membrane. In all cases considered here, it appears that there exists a critical value of the non-dimensional shear rate (the capillary number) above which no steady solution can be obtained, and where the capsule continuously deforms. This phenomenon is interpreted as the outset of burst. The model shows also the importance of the sphericity index for the determination of the overall capsule deformability.

1. Introduction

The term capsule has been proposed to designate a particle consisting of a thin elastic membrane enclosing a drop of a viscous incompressible Newtonian fluid. Depending on its specific properties (geometry, membrane mechanical behaviour, internal viscosity), a capsule may be viewed as a model for a variety of particles: liquid droplets, red blood cells, lipid vesicles, etc. Such particles deform when they are freely suspended in a flowing viscous fluid, and they may eventually break up if the shear rate is sufficiently large. It is of course important to be able to model those phenomena in order to study complex situations involving suspensions of capsules such as: behaviour in shear flow and rheology, filtration, human microcirculation, etc. Leaving aside eventual particle interactions, the problem thus consists in finding the motion and deformation of a capsule under the influence of the viscous fluid forces. It involves a free surface where the boundary conditions (continuity of velocity and balance of elastic and viscous forces) are applied, but the position of which is *a priori* unknown. Such problems are intrinsically nonlinear and furthermore the nonlinear theory of large elastic deformations must be used to model the wall mechanics. Consequently, the existing analytical solutions are very few and can be roughly divided in two groups: those that consider ellipsoidal capsules (Keller & Skalak 1982), but deal only very approximately with the membrane problem, and those that treat rigorously the membrane mechanics, but that are restricted to nearly spherical shapes (Barthes-Biesel & Chhim 1981; Barthes-Biesel & Rallison 1981). Although useful from the fundamental point of view, the latter results are of limited applicability to real situations, since they are restricted to small deformations and to initially spherical shapes (thus eliminating red blood cells or lipid vesicles). In order

to be able to depict more realistic situations, it is necessary to remove these restrictions, and to consider the large deformations of capsules of arbitrary initial shapes. This can be achieved only by means of a numerical model.

Using Ladyzhenskaya's (1963) integral solution to Stokes flow, Youngren & Acrivos (1976) developed a seemingly promising numerical technique to calculate the steady deformations of a gaseous droplet suspended in an extensional flow. Rallison & Acrivos (1978) extended these results to the case of a viscous liquid droplet in an extensional flow and predicted the breakup of the particle. These results have been also extended to general shear flows by Rallison (1981), when the interior and exterior fluid viscosities are equal. In this method, the Stokes equations of the problem are reformulated as an integral equation which is solved on the interface. The dimension of the problem is thus reduced.

It is the aim of the present paper to show that it is possible to adapt this technique to the more general case of capsules. To show the feasibility of the method, we model the motion and the deformation of an axisymmetric capsule with a Mooney–Rivlin type membrane, when it is suspended in an extensional flow, leaving three-dimensional flows for a future study. Large deformations are obtained, and the influence of the initial geometry and of the mechanical properties of the membrane is studied. A very interesting aspect of the model is that it can predict the burst of the capusle, without any specific hypothesis about a breakdown mechanism for the membrane material. Indeed, it appears that when the shear rate exceeds a critical value, no steady-state solution can be found and the capsule deforms continuously until of course it breaks. This is closely analogous to what is found for liquid droplets by Barthes-Biesel & Acrivos (1973) and numerically confirmed by Rallison & Acrivos (1978). This is the first time that burst of a capsule suspended in shear flow has been predicted. The present results may have interesting implications regarding the rupture of red blood cells (hemolysis) under shear, a well-known phenomenon.

The problem equations are presented in §2. The particular form of those equations in the axisymmetric case is given in §3. The numerical tests are developed in §4. The results regarding the main parameters influencing capsule deformability are discussed in §5.

2. Statement of the problem

Consider a capsule of known unstressed geometry (characteristic dimension d). The membrane is an infinitely thin sheet of an hyperelastic material (surface elastic modulus E_s) devoid of bending resistance. The internal medium is a Newtonian incompressible liquid of viscosity $\lambda\mu$. The particle is suspended into another Newtonian incompressible liquid of viscosity μ, subjected to a linear shear flow of magnitude G. There are no buoyancy effects. Non-dimensional quantities are used throughout: lengths are scaled by d, velocities by Gd, viscous stresses by μG and elastic tensions by E_s. From previous analytical studies of the deformation of a spherical capsule, it appears that the problem depends on two main parameters:

$$\Omega = \frac{\mu G d}{E_s}, \quad \lambda,$$

where Ω is the capillary number and represents the ratio of viscous to elastic forces, and where λ is the ratio of the interior to the exterior viscosity.

All motions are refered to a frame linked to the centre of mass **0** of the particle, and

having a translational motion with the velocity of the fluid at **0** with respect to a fixed set of axes.

The domains occupied by the internal liquid, the external liquid and the membrane are respectively denoted V^*, V and S. Assuming that the particle Reynolds number is very small, the fluid motion may be described by the Stokes equations:

$$\nabla\cdot\boldsymbol{v}=0, \quad \nabla\cdot\boldsymbol{\sigma}=0, \tag{2.1}$$

with

$$\boldsymbol{\sigma}=-p\boldsymbol{I}+\lambda(\nabla\boldsymbol{v}+\nabla\boldsymbol{v}^{\mathrm{T}}), \quad \text{in } V^*, \tag{2.2a}$$

$$\boldsymbol{\sigma}=-p\boldsymbol{I}+(\nabla\boldsymbol{v}+\nabla\boldsymbol{v}^{\mathrm{T}}), \quad \text{in } V. \tag{2.2b}$$

Two boundary conditions are expressed on the deformed surface:

$$[\boldsymbol{v}]_S=0, \tag{2.3}$$

$$\Omega[\boldsymbol{\sigma}\cdot\boldsymbol{n}]_S=-\boldsymbol{q}, \tag{2.4}$$

where $[\ ]_S$ denotes the jump of the bracketed quantity across S, and where $\boldsymbol{q}$ is the force per unit area of deformed surface exerted by the shell on the surrounding media. Its general expression may be found in Barthes-Biesel & Rallison (1981).

The last condition is expressed far from the particle:

$$\boldsymbol{v}\to\boldsymbol{v}^{\infty} \quad \text{as } |\boldsymbol{x}|\to\infty, \tag{2.5}$$

where $\boldsymbol{v}^{\infty}$ represents the undisturbed flow of the suspending fluid.

The full solution to these equations gives the instantaneous velocity of every point in space. It thus contains more information than is needed to determine the deformation of the capsule. A convenient formulation of the problem is as an integral equation where, as shown by Youngren & Acrivos (1976), the velocity $\boldsymbol{v}(\boldsymbol{x})$ of any point of the surface is given by an equation of the form

$$\tfrac{1}{2}(1+\lambda)\,\boldsymbol{v}(\boldsymbol{x})+(1-\lambda)\int_S[\boldsymbol{M}(\boldsymbol{x}-\boldsymbol{y})\cdot\boldsymbol{v}(\boldsymbol{y})]\cdot\boldsymbol{n}(\boldsymbol{y})\,\mathrm{d}A(\boldsymbol{y}) = \boldsymbol{v}^{\infty}(\boldsymbol{x})-\frac{1}{8\pi\Omega}\int_S\boldsymbol{J}(\boldsymbol{x}-\boldsymbol{y})\cdot\boldsymbol{q}(\boldsymbol{y})\,\mathrm{d}A(\boldsymbol{y}), \tag{2.6}$$

where the integration is performed over the surface, with the current point denoted $\boldsymbol{y}$ and where the kernels $\boldsymbol{M}$ and $\boldsymbol{J}$ are known functions of position.

This set of equations is very general, and may be used to describe the flow around any three-dimensional capsule in any shear flow satisfying the Stokes equations. However, in order to test the feasibility of the method, it was decided to solve the simple problem where both the flow and the capsule were axisymmetric.

3. Axisymmetric case, elongational flow

The undisturbed velocity field is assumed to be a purely elongational flow given in the fixed reference frame by

$$v_1^{\infty}=2x_1, \quad v_2^{\infty}=-x_2, \quad v_3^{\infty}=-x_3. \tag{3.1}$$

The capsule is further assumed to be also axisymmetric, to have a fore-and-aft symmetry, and to be oriented in such a way that its axis of revolution $\mathbf{0}x_1$ coincides with that of the flow. In what follows, it will be more convenient to work with cylindrical coordinates x, r, ϕ, where from now on x stands for x_1.

At steady state, owing to the symmetry of the problem, the membrane and the internal fluid are both at rest. Consequently, the final deformed shape of the capsule cannot depend on λ, and it is thus possible to choose any value for this parameter without loss of generality. It is particularly useful to select $\lambda = 1$, because then one term in the integral equation identically vanishes, and (2.6) becomes

$$\boldsymbol{v}(\boldsymbol{x}) = \boldsymbol{v}^{\infty}(\boldsymbol{x}) - \frac{1}{8\pi\Omega}\int_S \boldsymbol{J}(\boldsymbol{x}-\boldsymbol{y})\cdot\boldsymbol{q}(\boldsymbol{y})\,\mathrm{d}A(\boldsymbol{y}). \tag{3.2}$$

Of course, the value of the internal viscosity enters the problem insofar as it determines the time the capsule takes to reach steady state once the flow is started. Furthermore, as shown by Youngren & Acrivos (1975), the ϕ-dependency may be integrated out of (3.2):

$$\begin{vmatrix} v_x(\boldsymbol{x}) \\ v_r(\boldsymbol{x}) \end{vmatrix} = \begin{vmatrix} v_x^{\infty}(\boldsymbol{x}) \\ v_r^{\infty}(\boldsymbol{x}) \end{vmatrix} - \frac{1}{8\pi\Omega}\int_L \begin{vmatrix} J_{xx}(\boldsymbol{x}-\boldsymbol{y}) & J_{xr}(\boldsymbol{x}-\boldsymbol{y}) \\ J_{rx}(\boldsymbol{x}-\boldsymbol{y}) & J_{rr}(\boldsymbol{x}-\boldsymbol{y}) \end{vmatrix} \begin{vmatrix} q_x(\boldsymbol{y}) \\ q_r(\boldsymbol{y}) \end{vmatrix} \mathrm{d}s(\boldsymbol{x}), \tag{3.3}$$

where L represents the meridian curve of the surface and s the arclength along L. The expressions of the integrated kernels, given by those authors, are recalled in the Appendix.

The integrals in (3.3) are improper when $\boldsymbol{y} = \boldsymbol{x}$, but they may be shown to be convergent since the singularity is logarithmic. This singularity is dealt with as explained in the following. Let J_{xx}^{*} denote the asymptotic expression of J_{xx} when $\boldsymbol{y} \to \boldsymbol{x}$, with similar notations for the other components of $\boldsymbol{J}$. Then, after adding and subtracting the singularity, (3.3) may be rewritten as

$$\begin{aligned} \boldsymbol{v}(\boldsymbol{x}) = \boldsymbol{v}^{\infty}(\boldsymbol{x}) - \frac{1}{8\pi\Omega}\Bigg(& \int_L \begin{vmatrix} J'_{xx}(\boldsymbol{x}-\boldsymbol{y}) & J'_{xr}(\boldsymbol{x}-\boldsymbol{y}) \\ J'_{rx}(\boldsymbol{x}-\boldsymbol{y}) & J'_{rr}(\boldsymbol{x}-\boldsymbol{y}) \end{vmatrix} \mathrm{d}s(\boldsymbol{y}) \\ & + \left[\int_L \begin{vmatrix} J^{*}_{xx}(\boldsymbol{x}-\boldsymbol{y}) & J^{*}_{xr}(\boldsymbol{x}-\boldsymbol{y}) \\ J^{*}_{rx}(\boldsymbol{x}-\boldsymbol{y}) & J^{*}_{rr}(\boldsymbol{x}-\boldsymbol{y}) \end{vmatrix} \mathrm{d}s(\boldsymbol{y})\right] \cdot \begin{vmatrix} q_x(\boldsymbol{x}) \\ q_r(\boldsymbol{x}) \end{vmatrix} \Bigg), \end{aligned} \tag{3.4}$$

with

$$J'_{xx}(\boldsymbol{x}-\boldsymbol{y}) = J_{xx}(\boldsymbol{x}-\boldsymbol{y})\,q_x(\boldsymbol{y}) - J^{*}_{xx}(\boldsymbol{x}-\boldsymbol{y})\,q_x(\boldsymbol{x}), \quad \boldsymbol{x} \neq \boldsymbol{y}, \tag{3.5a}$$

$$J'_{xx}(\boldsymbol{x}-\boldsymbol{y}) = 0, \quad \boldsymbol{x} = \boldsymbol{y}. \tag{3.5b}$$

The second integral of (3.4) is computed analytically. The asymptotic expressions for $\boldsymbol{J}^{*}$ and for its integral over L are given in the Appendix. Because of the axisymmetry, it is convenient to label the membrane material points in a meridian plane by their arclength S (corresponding to coordinates X, R; $S = 0$ at $X = 0$) before deformation and to define their position after deformation by the arclength s (corresponding to coordinates x, r) which thus becomes the main position parameter. Then the components of the unit tangent and normal vectors $\boldsymbol{t}$ and $\boldsymbol{n}$ to the deformed profile are given by

$$t_x = n_r = \frac{\mathrm{d}x}{\mathrm{d}s}; \quad t_r = -n_x = \frac{\mathrm{d}r}{\mathrm{d}s}, \tag{3.6a,b}$$

and the principal curvatures of the meridian surface become

$$K_s = \left|\frac{\mathrm{d}\boldsymbol{t}}{\mathrm{d}s}\right|; \quad K_{\phi} = \frac{n_r}{r}. \tag{3.7a,b}$$

The membrane equations greatly simplify since the principal directions of strain and of stress at each point are along the meridian and the parallel curves.

Consequently, the deformation is conveniently defined in terms of the principal extension ratios λ_s and λ_ϕ given by

$$\lambda_s = \frac{ds}{dS}; \quad \lambda_\phi = \frac{r}{R}. \tag{3.8a,b}$$

It is obviously possible to choose any type of hyperelastic behaviour, but this paper treats only the case of a membrane that is a very thin sheet of an isotropic elastic solid, obeying a Mooney constitutive law, where the strain energy W per unit area of undeformed membrane material is given by

$$W = \tfrac{1}{6}(1-\psi')\,[\lambda_s^2+\lambda_\phi^2+(\lambda_s\lambda_\phi)^{-2}-3]+\tfrac{1}{6}\psi'[\lambda_s^{-2}+\lambda_\phi^{-2}+(\lambda_s\lambda_\phi)^2-3].$$

The parameter ψ' measures the nonlinearity of the material, and may vary between 0 and 1. A neo-Hookean (linear) material corresponds to $\psi' = 0$. Then the corresponding principal elastic stresses can be deduced from the classical theory of shell mechanics (Green & Adkins 1960)

$$\sigma_{ss} = \frac{1}{3\lambda_s\lambda_\phi}\left(\lambda_s^2-\frac{1}{\lambda_s^2\lambda_\phi^2}\right)[(1-\psi')+\lambda_\phi^2\psi'], \tag{3.9a}$$

$$\sigma_{\phi\phi} = \frac{1}{3\lambda_s\lambda_\phi}\left(\lambda_\phi^2-\frac{1}{\lambda_s^2\lambda_\phi^2}\right)[(1-\psi')+\lambda_s^2\psi'], \tag{3.9b}$$

together with the components of the elastic force exerted by the interface:

$$q_s = \frac{1}{\lambda_s^2}\left[\frac{d\sigma_{ss}}{ds}+\frac{1}{r}\frac{dr}{ds}(\sigma_{ss}-\sigma_{\phi\phi})\right], \tag{3.10a}$$

$$q_n = -(K_s\sigma_{ss}+K_\phi\sigma_{\phi\phi}), \tag{3.10b}$$

from which we deduce easily the value of these components along the (x, r)-axes:

$$q_x = q_s t_x + q_n n_x, \tag{3.11a}$$

$$q_r = q_s t_r + q_n n_r. \tag{3.11b}$$

4. Numerical procedure

The principle of the method consists in simulating the transient response of the capsule to a sudden start of the elongation flow, until a steady state is reached where the surface velocity vanishes at each point of the interface. A description of the numerical procedure has been given by Helmy (1983), and is briefly outlined here.

As shown on figure 1, the undeformed meridian curve is partitioned into N intervals by $N+1$ unequally spaced points $\boldsymbol{X}_0 \ldots \boldsymbol{X}_N$. If, at a given time t, their positions $\boldsymbol{x}_0 \ldots \boldsymbol{x}_N$ are known, it is straightforward from (3.6)–(3.11) to determine the local deformation of the membrane, the elastic stresses and the force (q_x, q_r) at each point $\boldsymbol{x}_i$. Then, the integral equation (3.4) gives a value of the velocity $\boldsymbol{v}_i$ at each collocation point, from which the next position of the material point $\boldsymbol{x}_i$ is obtained:

$$\boldsymbol{x}_i(t+\Delta t) = \boldsymbol{x}_i(t)+\boldsymbol{v}_i(t)\,\Delta t, \tag{4.1}$$

with

$$\boldsymbol{v}_i(0) = \boldsymbol{v}_i^\infty.$$

The process is stopped when the velocity is everywhere less than a given percentage of its local undisturbed value, or when the deformation appears to increase without limit.

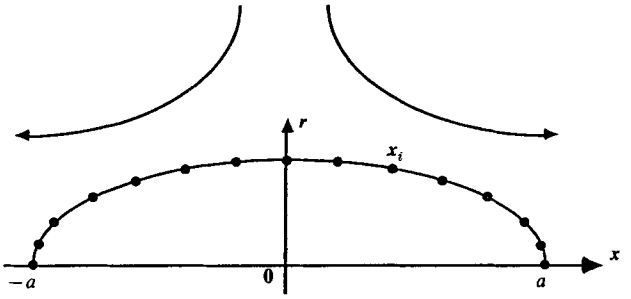

FIGURE 1. Axisymmetric capsule with fore-and-aft symmetry, suspended in an elongational flow. Non-equally-spaced collocation points are distributed on the membrane, and are followed along their displacement, during the deformation process.

The numerical derivations are performed with a five-unequally-spaced-point scheme, which gives fourth-order accuracy. Numerical integrals are computed with a Simpson type of procedure adapted to unequal intervals, which also gives fourth-order accuracy. The local tangent and normal vector components, as well as the curvature of the meridian line, are obtained directly from (3.6) and (3.7) by numerical derivations. The second curvature K_ϕ presents no difficulty except for the point $\boldsymbol{x}_N$ located on the axis of revolution, where it is simply set equal to the meridian curvature K_s. The principal elongation ratios λ_s and λ_ϕ are computed from (3.8). The value of λ_ϕ at $\boldsymbol{x}_N$ is set equal to that of λ_s.

The accuracy of the numerical calculation of $\boldsymbol{t}, \boldsymbol{n}, K_s$ and K_ϕ is tested for a sphere and for an ellipsoid with an aspect ratio of 4. With 30 equally spaced points along a half-meridian curve, the maximum error on the curvature is 0.2% for a sphere and 5% for the ellipsoid. In this last case it is possible to improve the accuracy by increasing the density of collocation points near the end. For example, starting with 27 equally spaced points, and adding 3 intermediate points in the last three intervals, reduces the error to less than 1% for the ellipsoid.

The procedure adopted in this paper to evaluate the contribution of the singularity gives better precision than the one used by Rallison & Acrivos (1978), which consists in replacing the contribution of $\boldsymbol{J}$ over the interval that contains the singularity by the analytical value of the integral of $\boldsymbol{J}^*$ over the same interval. The numerical integration of (3.4) and the procedure adopted to evaluate the singular contribution are validated by means of tests made on solid ellipsoids for which the expression for the viscous force $\boldsymbol{q}$ exerted by the external flow on the surface of the particle is given exactly by Jeffery (1922). Using this value in (3.4) and integrating, the resulting velocity on the surface of the particle should be everywhere zero. Table 1 shows the results of this test, made for a prolate spheroid of aspect ratio 4 with 31 evenly spaced collocation points. The computed velocity is given for different points of the profile, and it is everywhere less than 0.01% of its undisturbed value with our procedure, but about 1% with the procedure of Rallison & Acrivos. A problem arises, though, for the velocity computation at collocation point $N-1$. When $\boldsymbol{y} \to \boldsymbol{x}$, the function to be integrated has an $O(1)$ variation between points N and $N-1$, and this causes a large numerical error. (For example J'_{xx} varies from 0 at point $N-1$ to roughly $-4q_x(N-1)$ at point N). However, since both the values of the velocity at the end point and at point $N-2$ were satisfactory, the value of velocity at point $N-1$ was simply obtained by a linear interpolation between points $N-2$ and N.

	Present		Rallison & Acrivos	
I	$v_x(I)$	$v_r(I)$	$v_x(I)$	$v_r(I)$
0	0	0.4×10^{-4}	0	0.8×10^{-3}
1	0.2×10^{-6}	0.5×10^{-4}	0.3×10^{-4}	0.2×10^{-2}
15	0.3×10^{-5}	0.7×10^{-4}	0.4×10^{-3}	0.5×10^{-2}
29	0.5×10^{-4}	0.8×10^{-4}	0.8×10^{-2}	0.4×10^{-2}
30	0.6×10^{-4}	0	0.5×10^{-2}	0

TABLE 1. Numerical evaluation of the velocity at the Ith collocation point on the surface of a prolate solid spheroid with axis ratio 4. Comparison between the present treatment of the singularities and the method of Rallison & Acrivos.

Convergence is assumed when the membrane velocity is everywhere less than 2.5% of its undisturbed value. Numerical stability is ensured when

$$\Delta t < \Omega \Delta s.$$

This criterion leads to very small values of Δt, which hopefully may be increased with Ω. However, for a given repartition of collocation points, when Ω increases, λ_s and thus Δs also increase, and as a consequence the numerical precision of the scheme decreases. Indeed, an oscillatory behaviour of the various computed quantities appears. This oscillation, which has a half-wavelength equal to the collocation-point spacing, is of numerical nature and is due to the numerical derivations. Furthermore, as Δs increases, it becomes impossible to satisfy the convergence criterion. A possible remedy is of course to increase the number of collocation points, and to thus improve the numerical precision. The drawback is that the computation time t_I per iteration grows exponentially with N, (numerical tests show that $t_I \approx 0.02\exp(0.06N)$), and also that the time step must be decreased since Δs is decreased. We decided instead to smooth out the deformed positions of the collocation points at each iteration, with cubic spline functions. This operation does not distort the final result for the deformed steady shape of the capsule, since the solution obtained with numerical smoothing, as the true solution, satisfies the integral equation

$$0 = \boldsymbol{v}^{\infty} - \frac{1}{8\pi\Omega}\int_S \boldsymbol{J}(\boldsymbol{x}-\boldsymbol{y})\cdot\boldsymbol{q}(\boldsymbol{y})\,\mathrm{d}A(\boldsymbol{y}). \tag{4.2}$$

Since inertia effects are neglected, any solution of (4.2) is a steady deformed shape of the capsule such that all problem equations are satisfied. This is verified by comparing deformed-capsule profiles obtained with and without smoothing. It appears that the two solutions differ by less than 2%, which is within the convergence criterion.

The advantage of the smoothing procedure is that it limits the effect of the numerical errors due to derivation and allows convergence with fewer collocation points than would be necessary without smoothing. The price to pay though is the cost of smoothing which is also an exponential function of N, (the time t_{IS} per iteration with smoothing was found to be approximately given by $t_{IS} \approx 0.05\exp(0.07N)$).

Tests were run for a spherical capsule, with $N = 48$ collocation points (32 evenly spaced points, and a density of points multiplied by 4 near the axis of revolution).

Without smoothing, the scheme converges up to values of Ω roughly equal to 0.03 for which the maximum value of λ_s is 1.2. However, near burst, λ_s is roughly equal to 2.8, so that, to reach such deformed shapes, it would be necessary to divide the collocation point spacing by a factor between 2 and 3, and also to divide the time step by an equivalent factor. With smoothing, the number of points may be kept equal to 48. It follows that, as compared to the overall computation time with smoothing, the total computation time without smoothing is multiplied by a factor lying between 6 and 180 corresponding to a number of collocation points multiplied respectively by 2 or by 3.

5. Results and discussion

5.1. *Definition of deformation*

The overall deformation of an axisymmetric capsule with fore-and-aft symmetry can be estimated by means of the following expression:

$$D = \frac{a/A - b/B}{a/A + b/B},$$

where A, B are the semi-axes lengths along respectively $\mathbf{0x}$ and $\mathbf{0r}$ before deformation and a, b the corresponding lengths after deformation. This definition is a generalization of the classical one, introduced to measure the deformation of a sphere, and thus D varies between 0 (no deformation) and 1 (maximum deformation).

5.2. *Comparison with other results*

The moderate deformations of an initially spherical capsule, with a Mooney–Rivlin membrane material, have been computed and compared to the analytical solution of Barthes-Biesel & Chhim (1981) obtained with a regular perturbation technique valid to $O(\Omega^2)$. This comparison indicates a good agreement (within 10%) between the numerical results and the analytical ones as long as Ω is less than 0.01, and the deformation less than 10%. This condition may then be considered as the limit of validity of the asymptotic solution, which applies anyway only to moderate deformations of the particle.

A second test consists in comparing the present results to those obtained by E. J. Hinch (private communication), for a viscous liquid drop, with the same integral-equation formulation. These results seem to be more precise than those of Rallison & Acrivos (1978). The droplet can be considered as a capsule surrounded by a membrane with a constitutive strain–stress relation given by Laplace's law. The two solutions are shown on figure 2, where it appears that there is a very good agreement between them.

5.3. *Burst*

In all cases studied, it is found that when the flow strength, or equivalently Ω, increases, the deformation grows, until a critical value Ω_c is found, above which no steady state exists.

For values of Ω less than Ω_c a steady profile is obtained, the deformation of which increases with Ω (see figures 5, 8, 9). Figure 3 shows the variation with time of the meridional tension σ_{ss} evaluated at $x = 0$, for two values of Ω below and above Ω_c. When Ω is less than Ω_c, σ_{ss} reaches a finite steady value, whereas σ_{ss} increases without bound when Ω exceeds Ω_c. A similar behaviour for other quantities such as the elongation ratios, the membrane velocity, etc., is observed. It appears that for

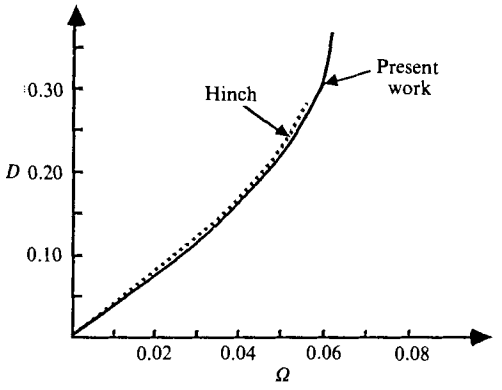

FIGURE 2. Deformation D of a liquid droplet as a function of capillary number Ω. Comparison between the results obtained by E. J. Hinch (private communication) and by the present model.

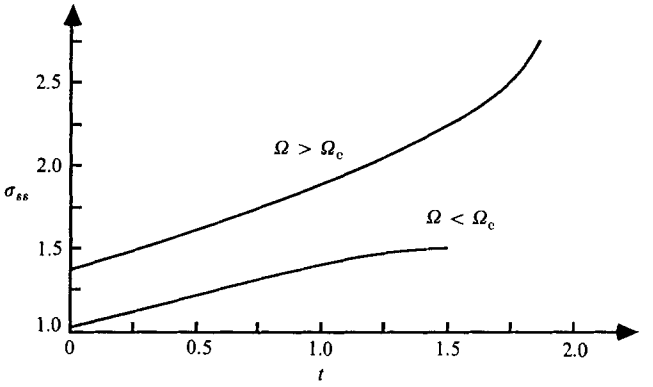

FIGURE 3. Meridional elastic tension σ_{ss} at the centre of the membrane ($x = 0$) as a function of time t. For values of capillary number Ω lower than Ω_c, a steady state is reached, whereas when $\Omega > \Omega_c$, the tension grows without bound until burst occurs, due to membrane mechanical failure.

	A	B	A/B	$< \Omega_c <$		λ_c
Ellipsoids	0.83	1.10	0.75	0.086	0.090	2.78
	1.00	1.00	1.00	0.083	0.086	2.75
	1.21	0.91	1.33	0.068	0.072	2.64
	1.59	0.79	2.00	0.057	0.062	2.32
Slugs	1.14	0.89	1.29	0.076	0.080	2.62
	1.16	0.87	1.33	0.074	0.078	2.60
Disks	0.77	1.08	0.71	0.092	0.096	2.71
	0.80	1.07	0.75	0.091	0.095	2.68

TABLE 2. Lower and upper bounds of the critical capillary number. The lower bound corresponds to the last steady profile obtained, with a maximum value of the meridional extension ratio λ_c. The upper bound corresponds to a capillary number for which the capsule deforms continuously.

values above Ω_c, the capsule continuously deforms until, of course, the membrane ruptures. The exact occurrence of burst depends on the mechanical properties of the wall material. The numerical model thus gives an estimate of the critical value of the shear rate when this phenomenon happens. On table 2 are shown lower and upper

			$V = \frac{4}{3}\pi$	
	A/B	K_s	A	B
Ellipsoids	0.75	0.985	0.83	1.10
	0.78	0.989	0.85	1.09
	1.00	1.000	1.00	1.00
	1.33	0.986	1.21	0.91
	2.00	0.929	1.59	0.79
	4.00	0.881	2.52	0.63
Slugs	1.29	0.986	1.14	0.89
	1.33	0.983	1.16	0.87
	1.92	0.929	1.44	0.75
Disks	0.71	0.985	0.77	1.08
	0.75	0.989	0.80	1.07

TABLE 3. Capsule geometrical characteristics. The last two columns give the corresponding values of the axes of the capsule which has the same volume as the unit sphere.

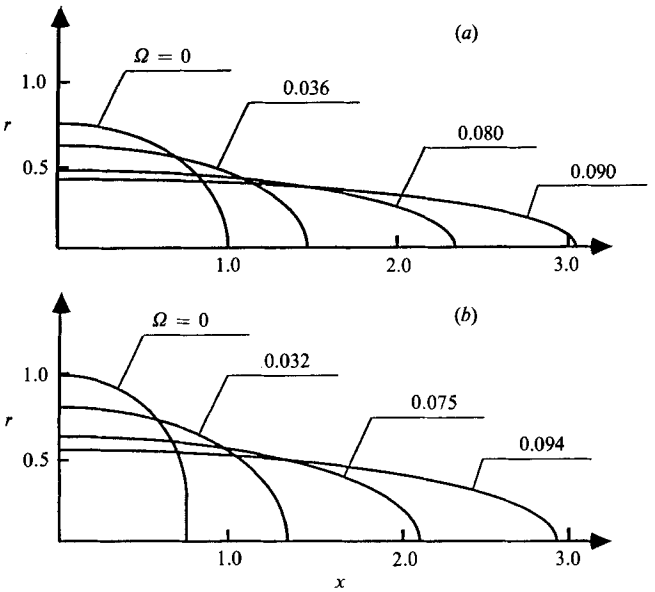

FIGURE 4. Successive steady deformed profiles of a capsule for increasing values of the capillary number Ω. (*a*) Prolate ellipsoid $A = 1.00$, $B = 0.75$. (*b*) Disk $A = 0.75$, $B = 1.00$. The oblate profile is deformed into a prolate one by flow.

bounds for Ω_c. The lower bound corresponds to the last steady profile obtained, whereas the upper bound corresponds to a situation where no steady shape could be obtained. The value of the maximum meridional extension ratio is also shown on table 2. It appears that near burst λ_s is of order 2.5, much less than the critical value commonly encountered for mechanical failure of an elastomer ($\lambda_s \approx 4$). For a liquid drop, this phenomenon of deformation and burst is well known and has been observed experimentally as well as modelled theoretically. Correspondingly, experimental observations show that when human red cells are subjected to a strong shear flow, they eventually burst. The model presented here predicts this behaviour.

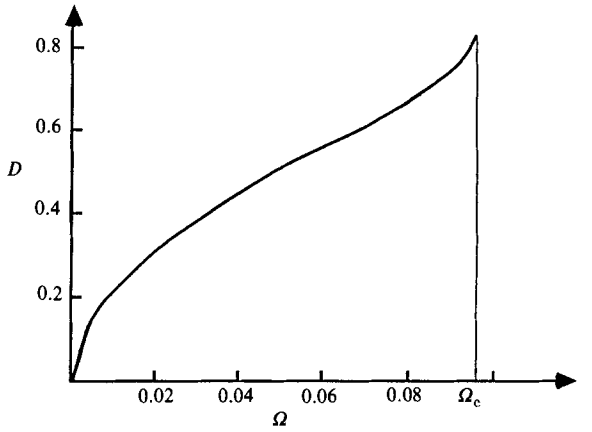

FIGURE 5. Deformation D of an oblate ellipsoid ($A = 0.75$, $B = 1.00$), as a function of capillary number Ω. For values of the capillary number higher than Ω_c, no steady deformation can be obtained.

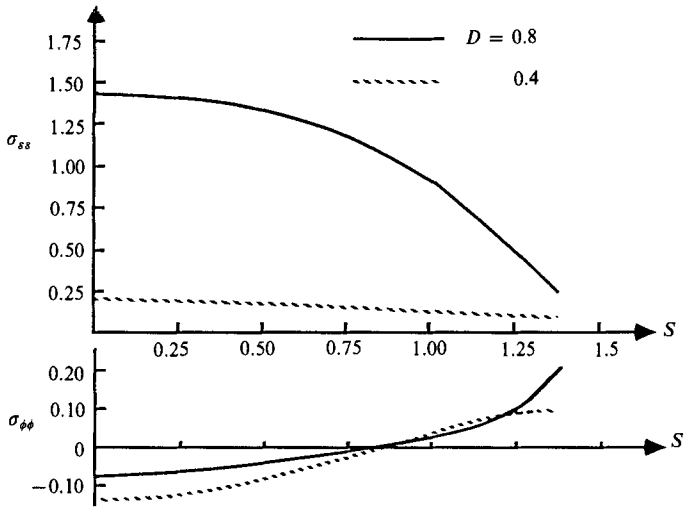

FIGURE 6. Meridional and transverse elastic tensions $\sigma_{ss}, \sigma_{\phi\phi}$, in the membrane, as functions of the initial arclength S for an oblate ellipsoid ($A/B = 0.75$). The capillary number is subcritical.

5.4. *Capsules with a neo-Hookean membrane*

For all capsules considered in this section, the membrane material is assumed to be neo-Hookean, but different initial geometries are studied: prolate and oblate ellipsoids, 'slugs' (cylinder closed by two hemispheres) and 'disks' (two parallel circular plates closed by a half torus). The influence of geometry is assessed by means of two parameters: the aspect ratio A/B and the so-called sphericity index K_s defined as follows:

$$K_s = \frac{\text{surface of the sphere of same volume}}{\text{surface of the particle}}.$$

The geometric characteristics of the different capsules are given in table 3, where the last two columns indicate the values of the semi-axes for a particle that has the same volume as a sphere of unit radius. The following discussion refers to isovolumic capsules.

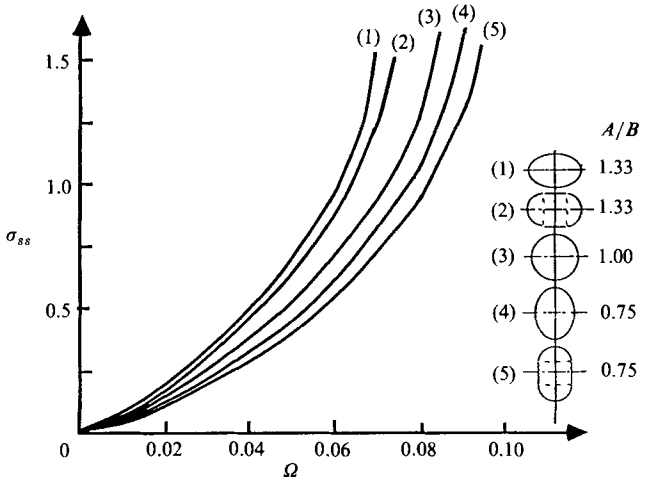

FIGURE 7. Values of the final steady meridional elastic tension σ_{ss} at $x = 0$, as a function of capillary number Ω, for capsules with different initial shapes.

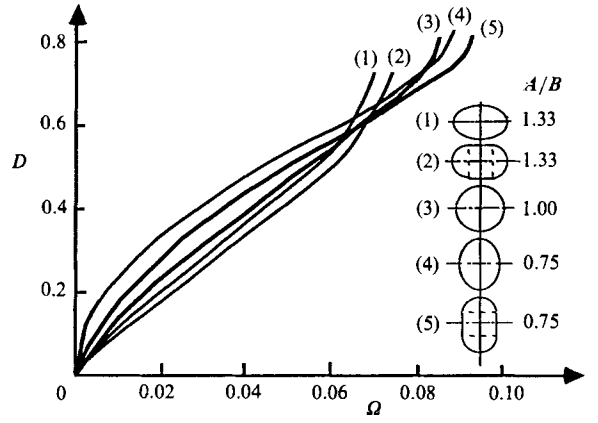

FIGURE 8. Deformation curves of isovolumic capsules. Capsules having the same initial aspect ratio A/B but different shapes behave differently.

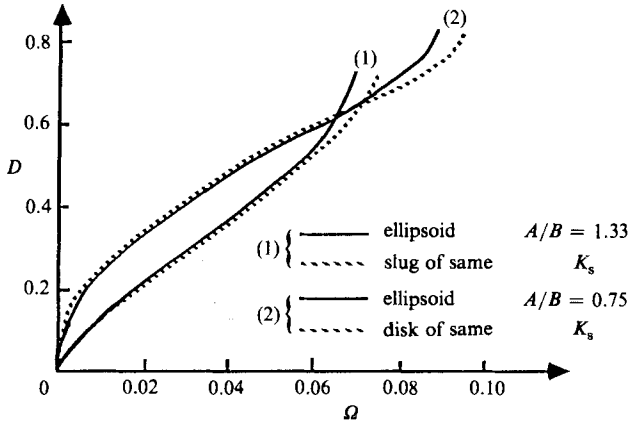

FIGURE 9. Deformation curves of isovolumic capsules. For the same value of the sphericity index K_s, the deformation curves are almost superimposed except near burst.

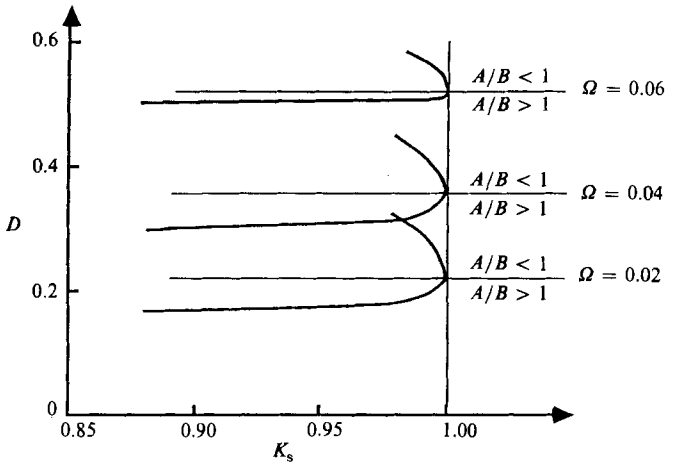

FIGURE 10. Effect of the sphericity index K_s on the deformation D for three different values of capillary number Ω. For oblate capsules ($A/B < 1$), a small variation in K_s creates a large change in D.

The successive steady deformed profiles of a prolate ellipsoidal capsule ($A = 1.00$, $B = 0.75$) and of a 'disk' ($A = 0.75$, $B = 1.00$) are shown on figure 4. It appears that the 'disk' transforms into a prolate profile, a fact which is consistent with observations of red blood cells suspended in shear flows. In both cases, the deformations are large, and the final profiles at high flow strengths are quite similar. In the case of an oblate ellipsoid ($A = 0.75$, $B = 1.00$), figure 5 shows that for increasing values of the flow strength, the deformation D increases and that, just before burst, it becomes quite large, of the order of 0.8.

In order to understand the mechanism of large deformations and of burst of the capsules, the stress distribution in the membrane and its time evolution have been analysed. For all capsules studied, the results are similar; they are illustrated for the case of an oblate ellipsoid ($A/B = 0.75$). Figure 6 shows the elastic-tension distribution along the meridian of the steady deformed membrane as function of the initial arclength S, for a relatively moderate deformation ($D = 0.4$) and near the burst limit ($D = 0.8$). In both cases, σ_{ss} is a decreasing function of S but is always positive. However, $\sigma_{\phi\phi}$ is first negative, representing a compressive force near the centre, then it becomes positive and represents an extensional force near the extremity. For $D = 0.8$, the ratio $\sigma_{ss}/\sigma_{\phi\phi}$ is of order 10 near the centre, and of order unity near the axis. Consequently the value of σ_{ss} governs the deformation and also the burst of the capsule, since membrane breakdown is linked to the maximum value of the tension in the structure. Figure 7 shows σ_{ss} at $x = 0$ where it is maximum, as function of Ω, for different capsules. Burst occurs when the slope of the curves increases sharply, and for values of σ_{ss} and λ_s respectively larger than 1.5 and 2.5.

The influence of geometry on the deformability is studied for isovolumic capsules characterized by their initial axis ratio. As shown on figure 8, capsules with the same initial aspect ratio A/B, but with different shapes have different deformation curves. For values of Ω, not too near Ω_c, D is an increasing function of the sphericity index K_s for prolate capsules, and a decreasing function for oblate ones. The deformations of two capsules having the same sphericity index K_s, but different initial shapes, are compared on figure 9 in the two cases where $A/B > 1$ or $A/B < 1$. It appears that

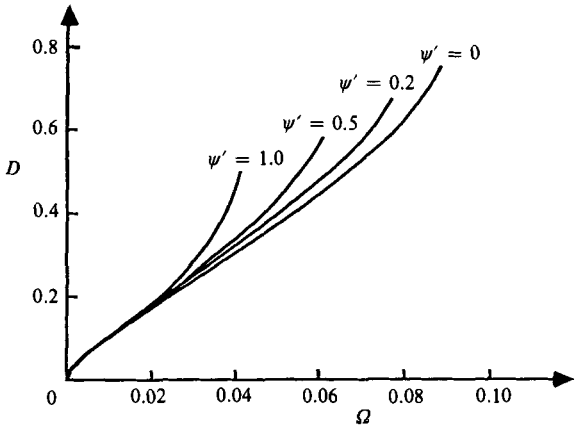

FIGURE 11. Influence of the membrane material properties on the deformation D of a prolate ellipsoid with aspect ratio $A/B = 1.33$. $\psi' = 0$ corresponds to a neo-Hookean material. As the nonlinearity of the material behaviour increases, the capsule deforms more readily, and burst occurs at lower values of Ω.

except near burst, the deformation depends mainly on K_s, and not on the exact initial geometry, provided the cases of prolate and oblate particles are distinguished. The variation of D with K_s for fixed values of Ω are shown on figure 10. For prolate capsules, D is not very sensitive to K_s. However, for oblate ones, small variations of K_s (less than 2%) result in large variations of D (more than 30%). It would then seem that K_s has a strong influence on the deformability of the capsule, as had been suspected for red blood cells.

When the capsules are near burst, the situation is more complex, and the sphericity index K_s cannot alone determine the deformation of the capsule, as shown on figure 9, where capsules of the same K_s, but of different shapes, have different values of Ω_c.

5.5. *Influence of the membrane material*

It is obvious that the constitutive law of the membrane material must also play an important role in the deformability of the capsule. For an hyperelastic membrane, the principal parameter is ψ' which measures the nonlinearity of the material. Figure 11 shows the influence of ψ' on the deformation of a prolate ellipsoidal capsule. For a given value of Ω, D is an increasing function of ψ', in agreement with Mooney's law, which predicts that, under the same load, the more nonlinear the material is, the more it deforms. A similar influence of ψ' exists for all capsules. One consequence is that the critical value of Ω becomes a decreasing function of ψ'.

5.6. *Variation of the membrane local surface area*

The question that arises now is the relevance of this study to biological capsules, such as red blood cells for example. It is known that membranes with a bilayer structure are essentially incompressible. This means that they deform in such a way as to maintain the local surface area constant. In terms of principal extension ratios, this condition leads to

$$\lambda_s \lambda_\phi = 1.$$

We have thus investigated the variation of the product $\lambda_s \lambda_\phi$ along the profile (figure 12) for different initial shapes but for the same value of the deformation ($D = 0.6$).

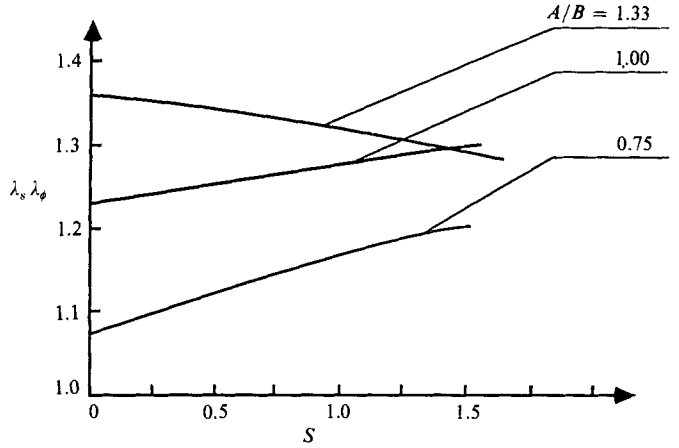

FIGURE 12. Evolution of the local area dilatation ($\lambda_s \lambda_\phi$) along the capsule profile, as a function of the initial arclength S of the capsule meridian. The area change is less important for an initially oblate capsule ($A/B < 1$).

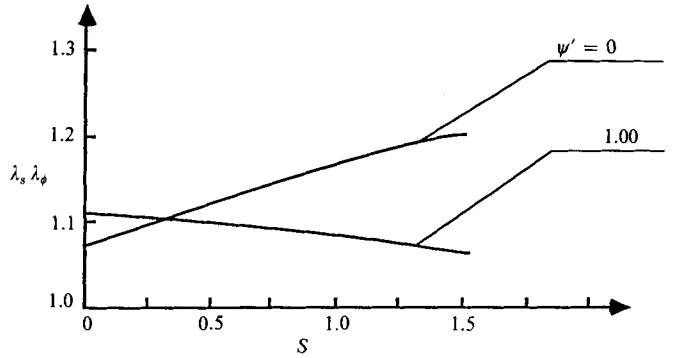

FIGURE 13. Influence of the membrane properties on the local area change for an oblate ellipsoidal capsule with aspect ratio $A/B = 0.75$. $\lambda_s \lambda_\phi$ measures the local area dilatation and S is the initial arclength on the meridian of the capsule.

It appears that $\lambda_s \lambda_\phi$ is always greater than unity and, although this is not shown on the figure, it increases with D. Consequently the capsule deforms with area dilatation and hence does not simulate satisfactorily the deformation of a red cell. Nevertheless, a comparison of the results obtained for a sphere and for two ellipsoids of aspect ratio 1.33 and 0.75, shows that for same deformation, the value of $(\lambda_s \lambda_\phi - 1)$ for the oblate ellipsoid is roughly half that of a sphere. Furthermore, according to figures 7 and 8, for the same Ω, the oblate ellipsoid with aspect ratio 0.75 has low values of σ_{ss}, but large values of D. This is consistent with the fact that the red cell that is discoidal in the undeformed state can easily reach large deformations without too significant internal tensions and with no area dilatation.

The curve obtained in the case where $\psi' = 1$ indicates the favourable influence of non-zero values of ψ' (figure 13).

6. Conclusion

As regards capsule mechanics, the numerical model developed here has provided some new informations, particularly on the mechanics of breakup. Indeed, it appears

that the burst of a capsule is due essentially to the non-existence of a steady equilibrium state between elastic and viscous forces, at least in the case of a Mooney–Rivlin membrane. Of course, the constitutive behaviour of the membrane material is important and it might be possible that a capsule with a shear-stiffening membrane would have a different behaviour. The model also shows the role of the sphericity index, which appears to be a very sensitive parameter governing capsule deformability.

The boundary-integral method seems well adapted to model the motion and the deformation of a capsule freely suspended in an elongational flow. It has been possible to study capsules having different initial shapes and to deform them considerably. Consequently, the generalization of the method to three-dimensional flows can be conceived.

The authors wish to thank E. J. Hinch and B. Duffy from the Department of Applied Mathematics and Theoretical Physics of Cambridge University for many fruitful discussions regarding the adaptation of their work on liquid drops to capsules. This research was supported in part by CNRS, ATP98358.

Appendix

Let $\boldsymbol{x}(x, R_x)$, $\boldsymbol{y}(y, R_y)$ be two points on the meridian of the capsule.

A.1. *Expressions for* J_{xx}, J_{xr}, J_{rx}, J_{rr} *(adapted from Youngren & Acrivos 1975)*:

$$J_{xx} = -2kR_x^{-\frac{1}{2}}R_y^{\frac{1}{2}}\left[F+\frac{E(x-y)^2}{R_{xy}^2}\right],$$

$$J_{xr} = k(x-y)\,R_x^{-\frac{1}{2}}R_y^{-\frac{1}{2}}\left[F-\frac{E(R_x^2-R_y^2+(x-y)^2)}{R_{xy}^2}\right],$$

$$J_{rx} = -k(x-y)\,R_x^{-\frac{3}{2}}R_y^{\frac{1}{2}}\left[F+\frac{E(R_x^2-R_y^2-(x-y)^2)}{R_{xy}^2}\right],$$

$$J_{rr} = -kR_x^{-\frac{3}{2}}R_y^{-\frac{1}{2}}\left[(R_x^2+R_y^2+2(x-y)^2)\,F - \frac{E(2(x-y)^4+3(x-y)^2(R_x^2+R_y^2)+(R_x^2-R_y^2)^2}{R_{xy}^2}\right],$$

where

$$k^2 = \frac{4R_xR_y}{(x-y)^2+(R_x+R_y)^2},$$

$$R_{xy}^2 = (x-y)^2+(R_x-R_y)^2,$$

$$E = \int_0^{\frac{1}{2}\pi}(1+k^2\sin^2\psi)^{\frac{1}{2}}\,\mathrm{d}\psi,$$

$$F = \int_0^{\frac{1}{2}\pi}\frac{\mathrm{d}\psi}{(1+k^2\sin^2\psi)^{\frac{1}{2}}}.$$

A.2. *Expressions for* $J^*_{xx}, J^*_{xr}, J^*_{rx}, J^*_{rr}$:

When $\boldsymbol{y} \to \boldsymbol{x}$, $x \neq a$ (a is the semi-axis of the capsule)

Let

$$F^* = \ln \frac{8R_x}{|s(x)-s(y)|},$$

$$J^*_{xx} = -2(F^* + t_x^2),$$

$$J^*_{rr} = -2(F^* - (2+t_x^2)),$$

$$J^*_{rx} = -K_\phi\{[s(x)-s(y)]F^* + 2R_x t_r\},$$

$$J^*_{xr} = K_\phi\{[s(x)-s(y)]F^* - 2R_x t_r\}.$$

When $\boldsymbol{y} \to \boldsymbol{x}$, $x = a$, only the value of J^*_{xx} is necessary for the calculation.

$$J^*_{xx} = -2\pi$$

A.3. *Analytical expressions for the integrals of* $J^*_{xx}, J^*_{xr}, J^*_{rx}, J^*_{rr}$ *over the meridian*:

When $x \neq a$, let

$$F^{**} = [s(a)+s(x)] \ln \frac{8R_x}{|s(x)+s(a)|} - [s(x)-s(a)] \ln \frac{8R_x}{|s(a)-s(x)|} + 2s(a),$$

$$G^{**} = -\tfrac{1}{2}[s(a)+s(x)]^2 \ln \frac{8R_x}{|s(x)+s(a)|} + \tfrac{1}{2}[s(x)-s(a)]^2 \ln \frac{8R_x}{|s(a)-s(x)|} - s(x)s(a),$$

$$\int_{-a}^{a} J^*_{xx}\,\mathrm{d}y = -2[F^{**} + 2s(a)\,t_x^2],$$

$$\int_{-a}^{a} J^*_{rr}\,\mathrm{d}y = -2[F^{**} - 2(2+t_x^2)\,s(a)],$$

$$\int_{-a}^{a} J^*_{xr}\,\mathrm{d}y = -K_\phi[G^{**} + 4R_x t_r s(a)],$$

$$\int_{-a}^{a} J^*_{rx}\,\mathrm{d}y = K_\phi[G^{**} - 4R_x t_r s(a)].$$

When $x = a$,

$$\int_{-a}^{a} J^*_{xx}\,\mathrm{d}y = -4\pi s(a).$$

REFERENCES

Barthes-Biesel, D. & Acrivos, A. 1973 Deformation and burst of a liquid droplet freely suspended in a linear shear flow. *J. Fluid Mech.* **61**, 1–21.

Barthes-Biesel, D. & Chhim, V. 1981 The constitutive equation of a dilute suspension of spherical microcapsules. *Intl J. Multiphase Flow* **7**, 493–505.

Barthes-Biesel, D. & Rallison, J. M. 1981 The time-dependent deformation of a capsule freely suspended in a linear shear flow. *J. Fluid Mech.* **113**, 251–267.

Green, A. E. & Adkins, J. C. 1960 *Large Elastic Deformation and Non-linear Continuum Mechanics*. Oxford University Press.

Helmy, A. H. 1983 Modélisations analytique et numérique du mouvement et de la déformation d'une capsule en suspension libre dans un écoulement. Application au globule rouge humain. Thèse Docteur Ingénieur, Université de Compiègne.

JEFFERY, G. B. 1922 On the motion of ellipsoidal particles immersed in a viscous fluid. *Proc. R. Soc. Lond.* A **102**, 162–179.

KELLER, S. R. & SKALAK, R. 1982 Motion of a tank-treading ellipsoidal particle in a shear flow. *J. Fluid Mech.* **120**, 27–47.

LADYZHENSKAYA, O. A. 1963 *The Mathematical Theory of Viscous Incompressible Flow.* Gordon and Breach.

RALLISON, J. M. 1981 A numerical study of the deformation and burst of a viscous drop in general shear flows. *J. Fluid Mech.* **109**, 465–482.

RALLISON, J. M. & ACRIVOS, A. 1978 A numerical study of the deformation and burst of a viscous drop in an extensional flow. *J. Fluid Mech.* **89**, 191–200.

YOUNGREN, G. K. & ACRIVOS, A. 1975 Stokes flow past a particle of arbitrary shape: a numerical method of solution. *J. Fluid Mech.* **69**, 377–403.

YOUNGREN, G. K. & ACRIVOS, A. 1976 On the shape of a gas bubble in a viscous extensional flow. *J. Fluid Mech.* **76**, 433–442.